Available online at www.sciencedirect.com
SCIENCE DIRECT
Polymer 46 (2005) 8796–8804
polymer
www.elsevier.com/locate/polymer

Non-isothermal crystallization of in situ polymerized poly(ε-caprolactone) functionalized-SWNT nanocomposites

Cynthia A. Mitchell, Ramanan Krishnamoorti*

Department of Chemical Engineering, University of Houston, 4800 Calhoun Ave., Houston, TX 77204-4004, USA

Received 24 November 2004; received in revised form 23 February 2005; accepted 13 May 2005
Available online 1 July 2005

Abstract

The non-isothermal crystallization behavior of three in situ polymerized, partially tethered poly(ε-caprolactone) with functionalized single walled carbon nanotube (SWNT) nanocomposites are examined using differential scanning calorimetry and corroborated using small and wide angle X-ray scattering. While the nanotubes are strong nucleators of the crystals of poly(ε-caprolactone) and dramatically accelerate the crystallization of the polymer, they do not alter the unit-cell, the melting temperature and the fractional crystallinity of the polymer crystals.

Keywords: Crystallization; Nanotube; Non-isothermal

1. Introduction

The extraordinary mechanical, transport and optical properties of single walled carbon nanotubes have attracted significant interest particularly towards their use in polymer nanocomposite materials [1]. However, one impediment for their use in such applications is their strong affinity for one another, making it difficult to disperse them as individual tubes [2]. Recently, the use of covalent [3] and non-covalent functionalization [4] and surfactant assisted solubilization [5] has provided possible mechanisms for the dispersion of SWNTs in polymer matrices. We have used covalently side-walled functionalized SWNTs for compatibilization with polystyrene matrices [6,7] and have used a similarly functionalized SWNT material for the development of end-tethered in situ polymerized poly(ε-caprolactone) nanocomposites [8]. In the case of the solution blended polystyrene nanocomposites we have observed the hydrodynamic manifestation of effective geometrical percolation for nanocomposites with 1.5 wt% functionalized nanotubes [6] while for the in situ polymerized nanocomposites the percolation threshold as observed by rheological measurements is lowered to below 0.35 wt% SWNTs [8]. In the case of the in situ polymerized poly(ε-caprolactone) nanocomposites the location of the percolation threshold implies an effective anisotropy of the dispersed SWNTs to be ~250 [8].

Previous studies of SWNTs and MWNTs dispersed in polypropylene [9,10], SWNTs in poly(vinyl alcohol) [11] and MWNTs in nylon-6 [12] have suggested that nanotubes can nucleate the crystallization of the matrix polymers. These observations are similar to those observed for layered silicate [13,14] and POSS based semi-crystalline polymer nanocomposites [15,16], where the increased interfacial area alters the kinetics and energetics of nucleation and growth, the overall crystallite fraction, and morphological organization, and at times even the unit cell structure and results in dramatic changes in the mechanical properties of the nanocomposite [17]. Finally, the tethering of nylon-6 chains to the surfaces of layered silicates along with their effective confinement between silicate sheets has shown the stabilization of a polymorph (γ-crystals as opposed to α-crystals) normally not considered to be stable at low temperatures [13].

In this study, we examine the influence of well-dispersed functionalized single walled carbon nanotubes that are used to co-initiate the polymerization of ε-caprolactone on the crystallization behavior of the matrix poly(ε-caprolactone) (PCL). The functionalization of the nanotubes were performed on small bundles of nanotubes and result in the

* Corresponding author. Tel.: +1 713 743 4312; fax: +1 713 743 4323.
E-mail address: ramanan@uh.edu (R. Krishnamoorti).

0032-3861/$ - see front matter © 2005 Elsevier Ltd. All rights reserved.
doi:10.1016/j.polymer.2005.05.101

placement, on an average, of ~1 functional group for every 65 C units of the SWNTs as described previously [6,8,18]. The prepared nanocomposites exhibit geometrically percolated filler network structures for nanotube loadings of 0.35 wt% or higher while at 0.2 wt% SWNT exhibits liquid-like behavior implying that the effective aspect ratio of the dispersed SWNTs are ~250 and indicating good dispersion. We present in this paper the non-isothermal crystallization and melting behavior as studied by differential scanning calorimetry and synchrotron based in situ simultaneous SAXS and WAXS on non-isothermally cooled and heated nanocomposites.

2. Experimental

The synthesis of the in situ polymerized nanocomposites has been described previously [8] and the materials characterization of the three nanocomposites and the extracted polymer are detailed in Table 1. The molecular weight and the fraction of polymer chains tethered to the nanotubes increased with increasing amount of SWNT in the nanocomposites. Since the molecular weight of the samples changed for each nanocomposite, each individual nanocomposite is compared directly to the corresponding extracted polymer in the studies reported here.

Simultaneous small-angle (SAXS) and wide-angle (WAXS) X-ray scattering experiments were conducted at the advanced polymers beamline (X27C) of the national synchrotron light source (NSLS), Brookhaven National Laboratory (BNL). The wavelength of the incident X-rays was 1.307 Å defined by a double multi-layer monochromator. Data were collected using two linear position sensitive detectors at 190 cm (SAXS) and 20 cm (WAXS). The scattering angle was calibrated using silver behenate (SAXS) and quartz (WAXS) powder samples. Samples, mounted in copper holders and encased between kapton® windows, were heated and cooled at heating rates of ~2 °C/min over a temperature range of 35–80 °C. Data acquisition times were typically 0.5 min. The data were corrected for indent beam fluctuations and normalized per sample transmission.

Deconvolution of the superposition of crystalline and amorphous peaks observed in the WAXS data was carried out using IgorPro. A linear baseline was used and the peak data fitted to Gaussian peaks. The analyses yielded integrated intensities, positions, heights and widths of the various reflections. The SAXS data were analyzed using the methodology outlined by Hsiao and co-workers [19].

Bulk differential scanning calorimetry (DSC) measurements were performed on a Perkin–Elmer Pyris 1 DSC instrument with sub-ambient capability. Non-isothermal heating and cooling calorimetric experiments on ~10 mg samples were performed from a temperature of 10–90 °C at heating and cooling rates of 5, 10, 15 and 20 °C/min.

Table 1
Sample characterization

Sample	SWNT (wt%)	M_w	M_w/M_n	% of PCL chains tethered
NC-A/poly-A	0.35	7200	1.6	36
NC-B/poly-B	1.8	12,700	1.4	57
NC-C/poly-C	4.6	18,600	1.7	72

3. Results and discussion

The heat flow DSC data for the non-isothermal crystallization at different cooling rates for a typical nanocomposite and the corresponding nanotube-free extracted polymer are presented in Fig. 1. The crystallization onset temperature (T_o), the crystallization end temperature (T_e) and the temperature corresponding to the peak in the crystallization

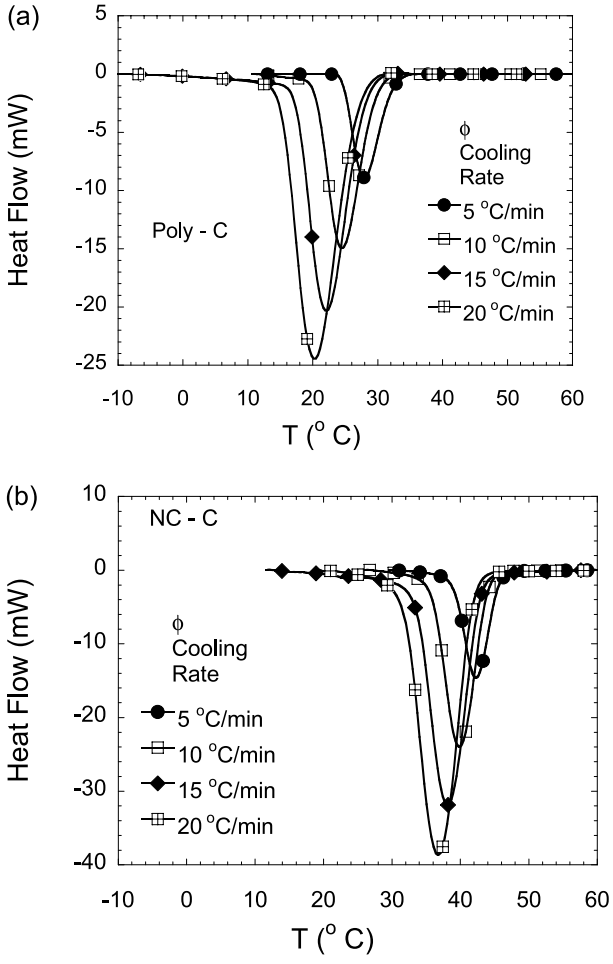

Fig. 1. Heat flow curves for the non-isothermal crystallization of (a) poly-C and (b) NC-C at four cooling rates from DSC measurements. The data clearly demonstrate the significant increase in the onset (T_o), end (T_e) and peak (T_p) crystallization temperatures for the nanocomposites as compared to their corresponding homopolymers and summarized quantitatively in Table 2a.

exotherm (T_p) are reported in Table 2a. There is a significant increase in the onset, peak and end crystallization temperatures for the three nanocomposites in comparison to their corresponding extracted polymers. Additionally, the difference between the polymer and the corresponding nanocomposite increases with increasing cooling rate. These non-isothermal crystallization results suggest that the nanotubes act as nucleating agents for the crystallization of poly(ε-caprolactone) chains [9,13,20].

Also reported in Table 2b are the total crystallization time (t_{crys}) for the polymer and the nanocomposites. These are calculated as

$$t_{crys} = \frac{T_o - T_e}{\phi} \tag{1}$$

where ϕ is the non-isothermal constant cooling rate. The values of t_{crys} are reduced for the nanocomposites as compared to their corresponding homopolymers for all heating rates and all loadings of SWNT. The lowered value for the t_{crys} implies that the time required for the crystallization process to be completed is somewhat lower for the nanocomposites and possibly suggests a decreasing time for the growth of the crystals in the presence of the SWNTs and possibly the effect of significantly increased nucleation density in the SWNT composites.

The kinetics of non-isothermal crystallization are interpreted using the relative crystallinity as a function of temperature, $X(T)$, defined as

$$X(T) = \frac{\int_{T_o}^{T} (dH/dT)dT}{\int_{T_o}^{T_e} (dH/dT)dT} \tag{2}$$

where H is the heat flow, was calculated for the non-isothermal DSC experiments. In the non-isothermal experiments described here the temperature is directly proportional to the cooling time ($t=(T_o-T)/\phi$) and an equivalent time dependent fractional crystallinity, $X(t)$, is defined. The relative crystallinity for the polymers and their nanocomposites are analyzed using the Avrami, Ozawa and a mixed Ozawa–Avrami model [16].

In the Avrami model, the time dependent crystallinity is modeled as

$$X(t) = 1 - \exp(-Z_t t^n) \tag{3a}$$

$$\log(Z_c) = \frac{\log(Z_t)}{\phi} \tag{3b}$$

where Z_t and Z_c are growth parameters and n is the Avrami exponent that takes on values between 1 and 4. Plots of $\log[-\ln(1-X(t))]$ and $\log(t)$ are shown in Fig. 2 for the 4.6 wt% SWNT nanocomposite and the extracted tube-free polymer. While the dependence shown in Fig. 2 is not linear over the entire range of crystallization time (or crystallinities), there is a region of crystallinity ($0.35 < X(t) < 0.75$) over which the modified Avrami analysis appears to be valid. The values of n, $t_{1/2}$ and Z_t obtained in those regions are tabulated in Table 3. Systematically, however, we note that the values of n and $t_{1/2}$ for the nanocomposites are a little lower than that of the polymer. Further, the values of Z_c (and Z_t) for the nanocomposites are somewhat larger than that for the polymers and that the differences become larger with decreasing cooling rate. While Z_t is a raw measure of the kinetics of crystallization (i.e. rate constant), Z_c attempts to quantify the crystallization rate constant after removing the kinetic effect of the non-isothermal cooling conditions under which the crystallization experiments are performed. These trends suggest that the inclusion of the nanotubes results in accelerating the kinetics of crystallization in these in situ polymerized nanocomposites.

The application of the Ozawa theory for non-isothermal crystallization kinetics is performed via

$$1 - X(T) = \exp\left[\frac{-k(T)}{\phi^m}\right] \tag{4a}$$

$$\log[-\ln(1 - X(T))] = \log(k(T)) - m\log(\phi) \tag{4b}$$

where m is the Ozawa exponent and $k(T)$ is a measure of the crystallization rate. The crystallization data on the basis of the Ozawa model are plotted in Fig. 3 and consistency with the Ozawa model (and Eq. (4b)) would require a linear relationship between $\log(-\ln(1-X(T)))$ and $\log(\phi)$. Clearly, while the homopolymers obey the Ozawa relationship, the nanocomposites do not follow Eq. (4) and large

Table 2a
Non-isothermal crystallization raw data parameters

Sample	Cooling rate											
	5 °C/min			10 °C/min			15 °C/min			20 °C/min		
	T_o (°C)	T_e (°C)	T_p (°C)	T_o (°C)	T_e (°C)	T_p (°C)	T_o (°C)	T_e (°C)	T_p (°C)	T_o (°C)	T_e (°C)	T_p (°C)
NC-A	42.8	35.6	39.7	41.0	33.6	37.3	39.8	31.4	35.6	38.9	29.5	34.2
Poly-A	35.4	28.2	32.6	33.3	24.9	29.3	31.6	22.4	27.3	30.6	20.4	25.8
NC-B	44.3	37.5	40.9	42.3	33.9	38.2	41.0	31.4	36.2	39.9	29.3	34.6
Poly-B	36.2	29.1	32.1	34.0	25.0	29.3	32.5	22.2	27.2	31.3	19.9	25.6
NC-C	45.7	38.8	42.3	44.0	35.7	39.9	43.0	33.4	38.2	41.9	31.6	36.8
Poly-C	32.3	24.7	28.2	29.6	20.5	24.8	28.0	17.4	22.3	26.8	15.1	20.6

Table 2b
Crystallization time

Cooling rate (°C/min)	t_{crys} (min)					
	Poly-A	NC-A	Poly-B	NC-B	Poly-C	NC-C
5	1.45	1.44	1.42	1.37	1.52	1.37
10	0.84	0.74	0.90	0.84	0.91	0.83
15	0.61	0.56	0.69	0.64	0.70	0.64
20	0.51	0.47	0.57	0.53	0.59	0.52

curvature is observed in the plots. Due to the low molecular weight of the PCL polymers considered here, secondary crystallization effects are less prominent and leads to the reasonable agreement with the Ozawa model in those cases. On the other hand, for the SWNT based nanocomposites, the presence of well-dispersed nanotubes results in instantaneous nucleation, rapid impingement and possibly secondary crystallization, and causes the failure of the Ozawa model. Since we observe a breakdown of the Ozawa model for the nanocomposites, we do not further analyze the data in the context of this model to extract the Ozawa exponent or crystallization rate parameters.

Liu has proposed the use of a combined Ozawa and Avrami model to describe the non-isothermal crystallization [16,21], with:

$$\log(\phi) = \log(F(T)) - b\log(t) \tag{5}$$

where $F(T)$ is the cooling rate to reach a defined degree of crystallization (and mathematically equal to $(k(T)/Z_t)1/m$)

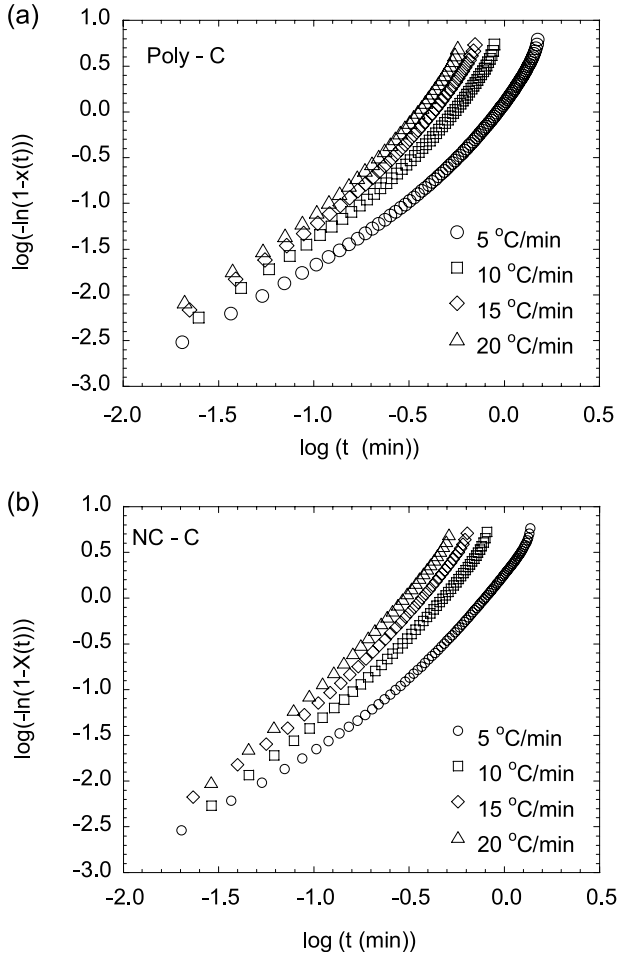

Fig. 2. Avrami analysis of the non-isothermal crystallization data for (a) poly-C and (b) NC-C. In both cases, the data as plotted here are non-linear demonstrating that the data cannot be fully analyzed using the Avrami model. However, a portion of the data corresponding to $0.35 < X(t) < 0.75$ was utilized to obtain the parameters reported in Table 3.

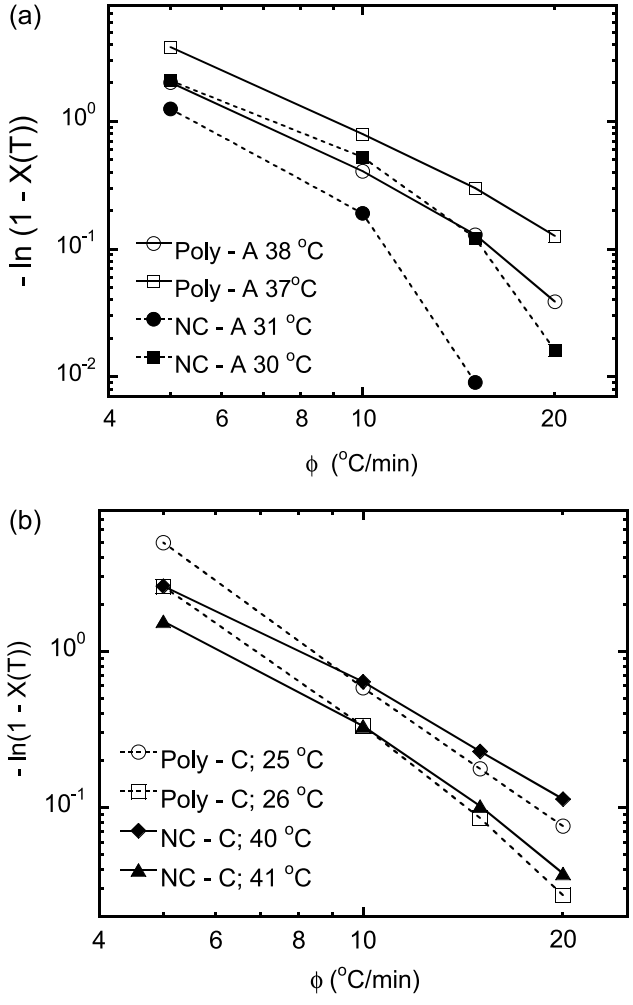

Fig. 3. Test of the Ozawa model to fit the crystallization data for (a) poly-A and NC-A and (b) poly-C and NC-C. In both cases the Ozawa model fails for the nanocomposites and works reasonably to represent the crystallization of the relatively low molecular weight pure polymers.

Table 3
Avrami analysis

Sample	Cooling rate															
	5 °C/min				10 °C/min				15 °C/min				20 °C/min			
	n	Z_t	Z_c	$t_{1/2}$ (min)	n	Z_t	Z_c	$t_{1/2}$ (min)	n	Z_t	Z_c	$t_{1/2}$ (min)	n	Z_t	Z_c	$t_{1/2}$ (min)
NC-A	2.1_0	2.2	1.17	0.62	2.1_6	7.6	1.23	0.37	2.1_6	13.8	1.19	0.28	2.2_0	21.6	1.17	0.23
Poly-A	2.3_8	1.6	1.09	0.68	2.3_9	5.3	1.18	0.39	2.3_2	10.6	1.17	0.28	2.3_1	17.4	1.15	0.23
NC-B	2.4_1	1.8	1.12	0.68	2.3_9	5.8	1.19	0.41	2.3_5	10.7	1.17	0.31	2.3_9	17.7	1.15	0.26
Poly-B	2.6_0	1.4	1.08	0.76	2.5_3	4.8	1.17	0.46	2.4_6	9.4	1.16	0.35	2.4_1	14.8	1.14	0.28
NC-C	2.4_4	1.8	1.12	0.68	2.4_3	6.1	1.20	0.41	2.4_0	10.9	1.17	0.32	2.3_9	18.7	1.16	0.25
Poly-C	2.5_9	1.2	1.04	0.80	2.5_3	4.7	1.17	0.47	2.5_6	9.1	1.16	0.37	2.5_7	14.8	1.14	0.30

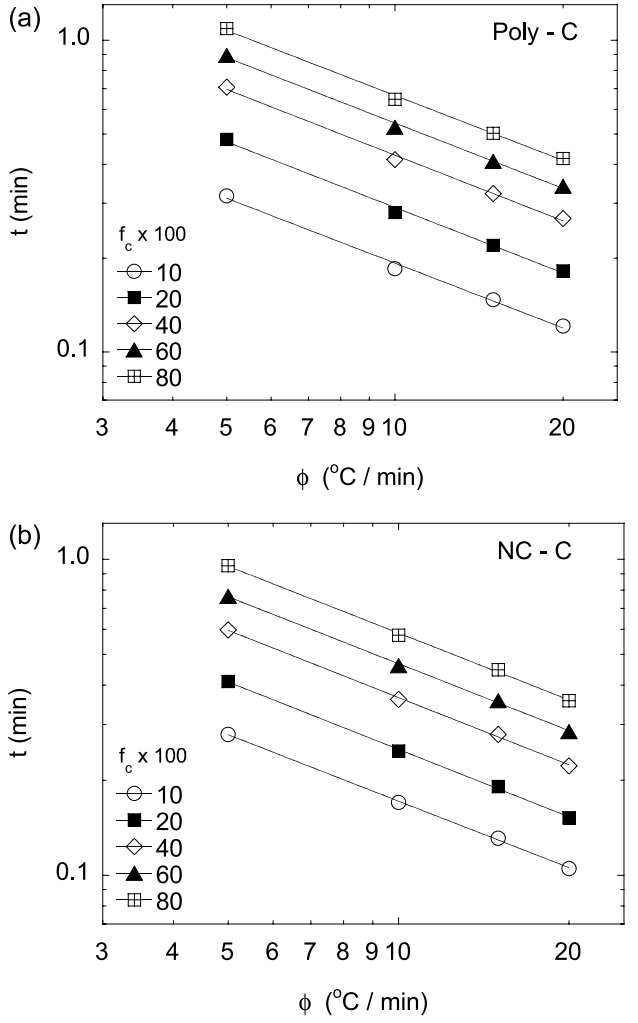

Fig. 4. Test of the Ozawa–Avrami model for the crystallization data of (a) poly-C and (b) NC-C.

and b is the ratio of the Avrami and Ozawa exponents. The data for both the polymers and the nanocomposites agree reasonably well with this model as shown in Fig. 4. The value of b and $F(T)$ are summarized in Table 4. The $F(T)$ value for the nanocomposites are generally smaller than those for the polymer and indicate that the nanocomposites achieve a value for the fractional crystallinity faster than the polymer, implying faster kinetics of crystallization, and consistent with our previous observation that the nanotubes act as nucleating agents.

An activation energy (E_a) for the non-isothermal growth of the crystals is determined using the Kissinger model as [22]:

$$E_a = -R\frac{d(\ln(\phi/T_p^2))}{d(1/T_p)} \tag{6}$$

and the values of E_a are tabulated in Table 5. From the data presented, it is clear that the presence of SWNTs does not lead to a substantial change in the value of E_a, especially with the value for the three nanocomposites not showing

Table 4
Combined Avrami–Ozawa analysis

Sample	$X(T)\times 100$							
	20		40		60		80	
	b	$F(T)$	b	$F(T)$	b	$F(T)$	b	$F(T)$
NC-A	1.36	0.11	1.37	0.33	1.38	0.48	1.39	0.61
Poly-A	1.30	0.17	1.27	0.41	1.27	0.56	1.27	0.69
NC-B	1.41	0.15	1.43	0.37	1.44	0.52	1.44	0.66
Poly-B	1.28	0.28	1.32	0.43	1.35	0.61	1.40	0.72
NC-C	1.41	0.15	1.41	0.38	1.42	0.53	1.42	0.67
Poly-C	1.42	0.24	1.42	0.48	1.43	0.62	1.44	0.75

any systematic dependence with the SWNT amount. It is suggested that the presence of SWNTs perhaps increases the activation energy (for the transport of PCL chains to the growing crystal) by a small amount. This would be consistent with a weak attraction between the nanotubes and the polymer segments as indicated by the dispersability of the SWNTs in the monomer (ε-caprolactone) [23].

On the other hand, the nucleation activity of the SWNTs in these nanocomposites is obtained by examination of the crystallization data using the method suggested by Dobreva, where [24]:

$$\log(\phi) = C - \frac{B}{2.303\Delta T_p^2} \tag{7}$$

where ΔT_p is the undercooling at the peak (i.e. $\Delta T_p = T_m - T_p$) and B is a parameter that is related to thermodynamic parameters as

$$B = \omega \frac{\sigma^3 V_m^2}{3kT_m(\Delta S_m)^2 n} \tag{8}$$

where V_m is the molar volume, ΔS_m the entropy of fusion, σ is the specific surface energy and ω is a geometrical constant. The nucleation activity, ε, is given as

$$\varepsilon = \frac{B_{NC}}{B_{Poly}} \tag{9}$$

with an ε of 0 indicating strong nucleation activity and ε of 1 indicating inert nanoparticle activity. The values of ε for the three nanocomposites (with respect to the corresponding nanotube extracted polymers) are 0.56, 0.47 and 0.23 for the 0.35, 1.8 and 4.6 wt% SWNT (NC-A, NC-B and NC-C) nanocomposites, respectively. These values suggest that with increasing SWNT concentration the nucleation activity afforded, in such non-isothermal measurements, by the SWNTs increases. This trend in ε is consistent with acceleration in the crystallization kinetics noted previously (for e.g. the increased value of Z_t for the nanocomposites in the Avrami model and the smaller value of $F(T)$ for the nanocomposites in the combined Ozawa–Avrami model).

Table 5
Activation energy from Kissinger analysis

Sample	E_a (kJ/mol)
NC-A	207.5
Poly-A	160.5
NC-B	182.3
Poly-B	166.7
NC-C	211.0
Poly-C	138.7

The results of the melting behavior following each of the non-isothermal crystallization experiments are summarized in Fig. 5 and Table 6. The melting temperatures for the nanocomposites are typically higher as compared to their respective unfilled polymers at all heating rates. The slight increase in the melting point might result from the superior thermal conductivity or the inherent attraction between the polymer and the SWNTs leading to a stabilization of the crystalline phase. Further the extent of crystallinity (and reported as f_c), obtained assuming that 100% crystalline PCL has an enthalpy of melting of 139.3 J/g [25], are roughly similar for the polymers and the nanocomposites with the values of f_c decreasing with increasing matrix molecular weight of the polymer. We suggest that while the nanotubes significantly affect the nucleation rate and that the spherulite sizes are significantly reduced due to the high density of nucleation sites, the lamellar thickness is

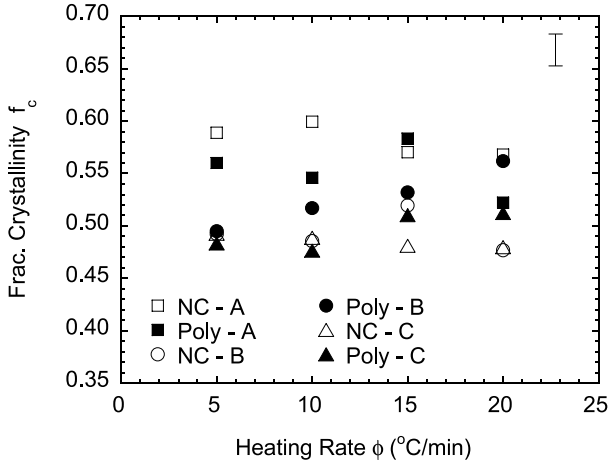

Fig. 5. Fractional crystallinity obtained by the measurement of the melting enthalpy after the non-isothermal crystallization experiments and normalized by the value for pure fully crystallized PCL. The data indicate no substantial change in the fractional crystallinity amongst the different nanocomposites and their respective extracted homopolymers.

Table 6
Melting characteristics following non-isothermal crystallization

Sample	Cooling rate (°C/min)							
	5		10		15		20	
	T_m (°C)	f_c	T_m (°C)	f_c	T_m (°C)	f_c	T_m (°C)	f_c
NC-A	54.9	0.59	55.1	0.60	55.6	0.57	56.5	0.57
Poly-A	53.0	0.56	54.3	0.55	54.7	0.58	55.1	0.52
NC-B	56.8	0.49	57.5	0.49	57.8	0.52	58.4	0.48
Poly-B	54.2	0.49	55.9	0.52	56.4	0.53	56.9	0.56
NC-C	57.5	0.49	57.8	0.49	58.6	0.48	59.3	0.48
Poly-C	55.3	0.48	55.1	0.48	55.2	0.51	55.5	0.51

largely unaffected (as proven below from X-ray measurements) and thus leads to largely unchanged values of f_c and T_m. We anticipate that if we go to still higher values of nanotube concentration, the nucleation density and the effective confinement of the polymer crystals should lead to a decrease in f_c and T_m.

While the non-isothermal crystallization experiments and the subsequent melting experiments provide us a macroscopic measure of the kinetics and extent of crystallization, they do not lend any insight into the molecular level and supermolecular organization of the polymers in the nanocomposites systems. To address this we performed simultaneous SAXS and WAXS measurements on samples heated and cooled non-isothermally at a heating/cooling rate of 2 °C/min were conducted. Some representative time/temperature data during the cooling experiments for both the SAXS and WAXS measurements are presented in Fig. 6. While in the WAXS data the peaks corresponding to the different crystallographic planes are readily observed as peaks riding on top of the amorphous halo, the SAXS data demonstrate the development of dramatically increased low angle scattering. The peaks in the WAXS data are consistent with the previously established crystallographic data for PCL and suggest that the addition of the nanotubes does not alter the unit cell structure of PCL. We note in this context that some of the chains of the PCL are tethered to the nanotube bundles with a maximum density of grafting that is evaluated as being approximately one polymer chain every five exposed carbon atoms of the SWNT bundles. Additionally the fractional crystallinity, f_c, was obtained as a function of temperature from the WAXS data as

$$f_c = \frac{A_{crys}}{A_{crys} + A_{amor}} \tag{10}$$

and shown in Fig. 7 as a function of temperature. Similarly, from the SAXS data an invariant was calculated as

$$Q = \int_0^\infty ([I(q) - I_{melt}(q)]q^2)\mathrm{d}q \tag{11}$$

and the changes in Q during the non-isothermal crystallization are reported in Fig. 8. The SAXS and WAXS data indicate that the time dependent non-isothermal crystallization behavior for the three nanocomposites is similar, and these results are similar to those observed previously using the DSC measurements.

In addition, from the SAXS measurements we estimate the long spacing L_b for the non-isothermal crystallization experiments by fitting the small angle peak data to a

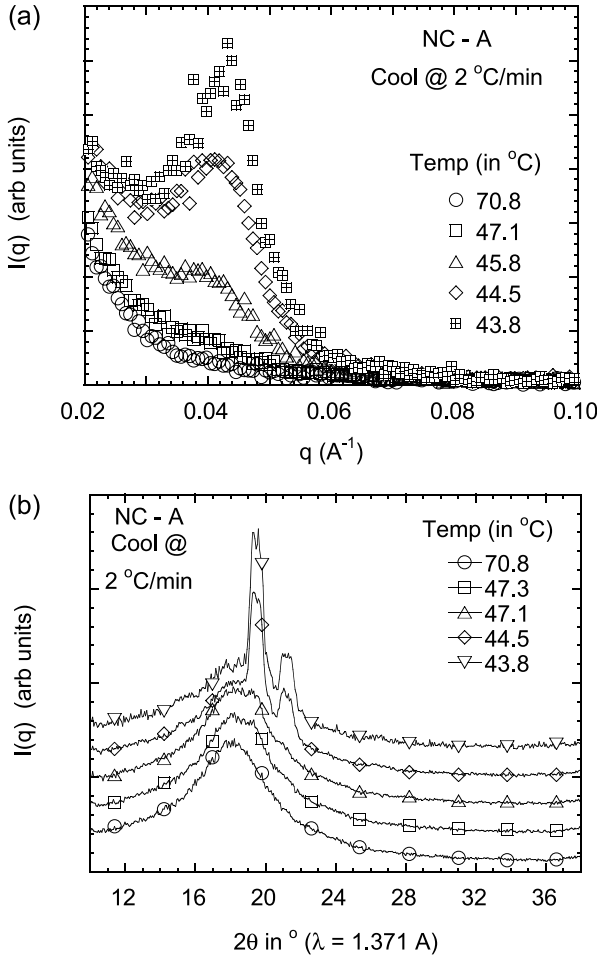

Fig. 6. SAXS (a) and WAXS (b) snapshots during the non-isothermal cooling experiment for the NC-A sample at select temperatures. In the SAXS data the monotonic data of the melt-state (amorphous) leads to the development of a low-angle peak. On the other hand, in the WAXS data the broad amorphous halo from the melt state demonstrates the development of sharp diffraction peaks corresponding the PCL crystal. We note that the peak assignments are consistent with the previous assignment of PCL crystal peaks.

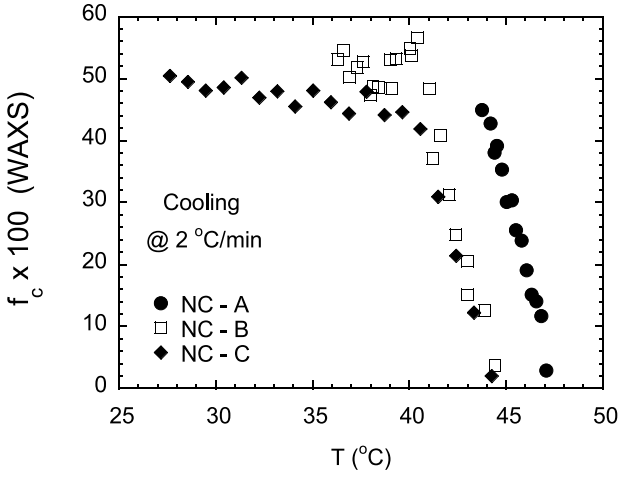

Fig. 7. The fractional crystallinity obtained from WAXS data using Eq. (10) for the non-isothermal cooling experiments for the three nanocomposites.

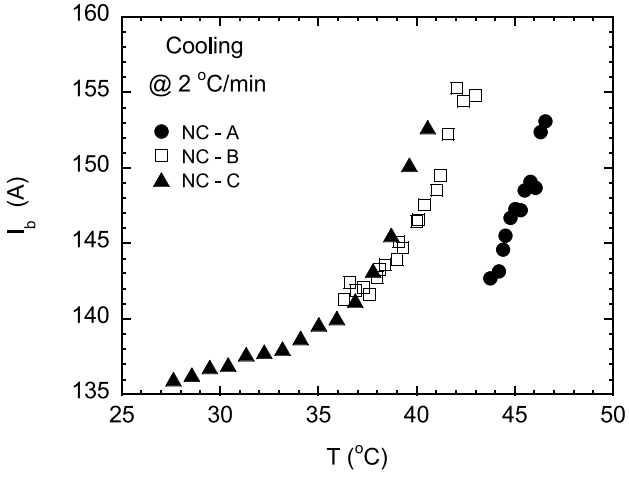

Fig. 9. The long spacing, L_b, obtained from the SAXS data reveals that the three nanocomposites are quite similar to each other.

Gaussian model and the peak value assigned as q^*, with

$$L_b = \frac{2\pi}{q^*} \tag{12}$$

The temperature dependence of L_b during the non-isothermal crystallization experiments for the three nanocomposites is shown in Fig. 9. These data indicate that L_b decreases with decreasing temperature and consistent with previous data for other crystalline polymers and their nanocomposites. Additionally, the data for NC-B and NC-C are similar and appear to suggest that the addition of the carbon nanotubes to the polymer does not significantly decrease the thickness of the lamellae and is consistent with the observed independence of fractional crystallinity and melting temperature with nanotube addition noted earlier.

Finally, the non-isothermal melting following the crystallization measurements were followed using SAXS and WAXS measurements and the fractional crystallinity

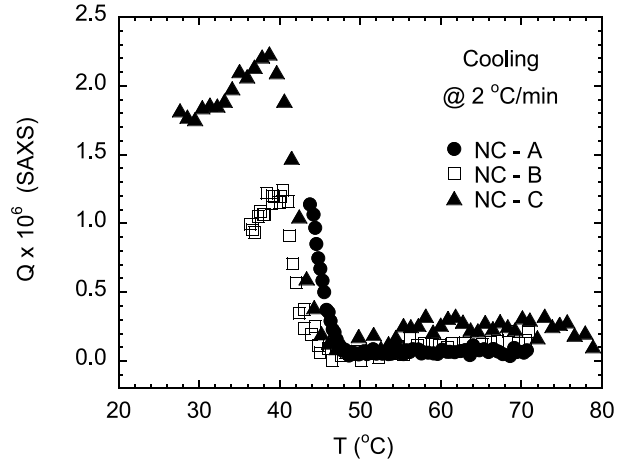

Fig. 8. The invariant calculated using Eq. (11) for the non-isothermal cooling SAXS data for the three nanocomposites. The results from the invariant analysis are similar to that obtained from the WAXS measurements.

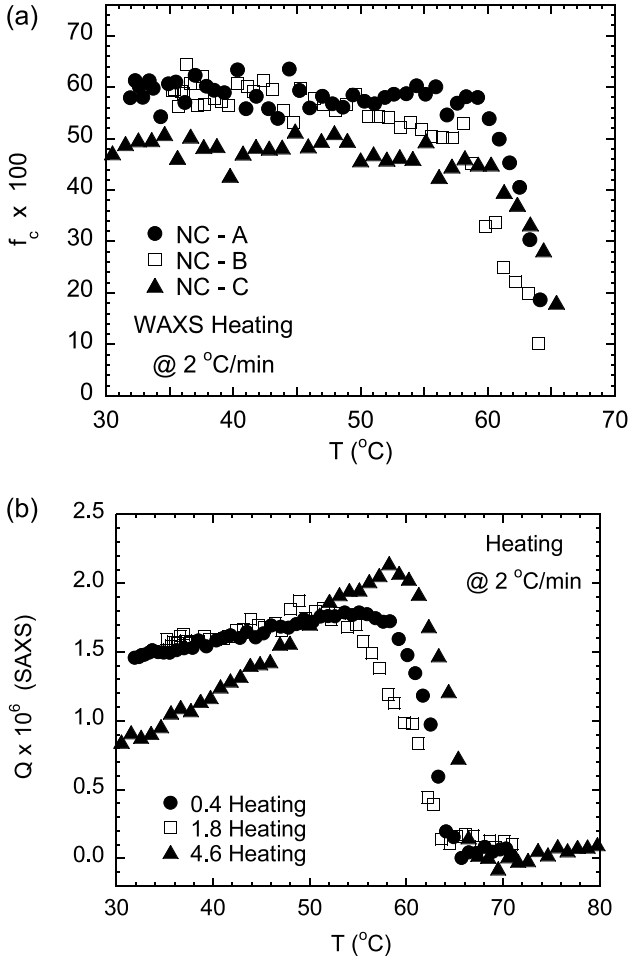

Fig. 10. The fractional crystallinity, f_c; (a) and the invariant, Q; (b) as a function of temperature during the heating following the non-isothermal crystallization measurements. The data suggests that the three samples are quite similar and that the melting character is essentially identical for the three nanocomposites.

(f_c) and the invariant (Q) are shown in Fig. 10. These results are consistent with the DSC results presented earlier that indicate that the melting characteristics of the three nanocomposites are virtually identical. Clearly the presence of a considerable fraction of polymer chains tethered to the nanotube bundle does not significantly alter the nature of the crystalline lamellae and only appears to considerably alter the size of the spherulites of the crystals. We anticipate that the confinement provided by the nanotubes along with the favorable interactions between the polymer and the nanotubes will result in change in the crystalline structure only at significantly higher loadings of nanotube concentration due to the nanoscale diameter of the nanotubes and the one-dimensionality of the nanotubes.

4. Concluding remarks

The non-isothermal crystallization of poly(ε-caprolactone) polymerized in the presence of functionalized single walled carbon nanotubes indicates that the nanotubes are efficient nucleators of PCL. However, these dispersed and functionalized nanotubes (and tethering of some of the chains to the SWNTs) do not lead to a change in the unit cell, melting point and the fractional crystallinity over the range of SWNT concentrations studied. Interestingly, we find that all three nanocomposites, with SWNT loadings varying from 0.35 to 4.6 wt% are not significantly different and the nucleation activity associated with the nanotubes only increasing weakly with nanotube concentration. We are currently examining the consequences of the dispersed nanotube bundles on the isothermal crystallization properties of PCL as well as structurally via Raman and atomic force microscopy methods.

Acknowledgements

We thank Prof Jim Tour and Dr Jeff Bahr for the functionalized SWNTs. Air Force Research Laboratory generously donated time on X27C at the NSLS at Brookhaven National Laboratory. We thank Dr Carlos Avila Orta and Dr Igor Sics for help at the NSLS at Brookhaven National Laboratory. Support of the Texas Institute for Intelligent Bio-Nano Materials and Structures for Aerospace Vehicles, funded by NASA Cooperative Agreement No NCC-1-02038 is gratefully acknowledged. CAM thanks NASA for partial funding through the Graduate Student Researchers Program.

References

[1] Ajayan PM, Charlier J-C, Rinzler AG. Proc Natl Acad Sci 1999; 96(25):14199–200. Saito R, Dresselhaus G, Dresselhaus MS. Physical properties of carbon nanotubes. London: Imperial College Press; 1998.
[2] Ausman KD, Piner R, Lourie O, Ruoff RS, Korobov M. J Phys Chem B 2000;104(38):8911–5.
[3] Bahr JL, Mickelson ET, Bronikowski MJ, Smalley RE, Tour JM. Chem Commun 2001;193–4.
[4] Star A, Liu Y, Grant K, Ridvan L, Stoddart JF, Steuerman DW, et al. Macromolecules 2003;553–60.
[5] Yurekli K, Mitchell CA, Krishnamoorti R. J Am Chem Soc 2004; 126(32):9902–3.
[6] Mitchell CA, Bahr JL, Arepalli S, Tour JM, Krishnamoorti R. Macromolecules 2002;35:8825–30.
[7] Pham JQ, Mitchell CA, Bahr JL, Tour JM, Krishanamoorti R, Green PF. J Polym Sci, Part B: Polym Phys 2003;41(24):3339–45.
[8] Mitchell CA, Bahr JL, Jeon K, Tour JM, Krishanamoorti R. Submitted for publication.
[9] Grady BP, Pompeo F, Shambaugh RL, Resasco DE. J Phys Chem B 2002;106(23):5852–8.
[10] Moore EM, Ortiz DL, Marla VT, Shambaugh RL, Grady BP. J Appl Polym Sci 2004;93(6):2926–33. Seo MK, Park SJ. Macromol Mater Eng 2004;289(4):368–74.
[11] Zhang X, Liu T, Sreekumar TV, Kumar S, Moore VC, Hauge RT, et al. Nano Lett 2003;3(9):1285–8. Probst O, Moore EM, Resasco DE, Grady BP. Polymer 2004;45(13):4437–43.
[12] Liu T, Phang IY, Shen L, Chow SY, Zhang W-D. Macromolecules 2004;37:7214–22.
[13] Lincoln DM, Vaia RA, Krishnamoorti R. Macromolecules 2004; 37(12):4554–61.
[14] Fornes TD, Paul DR. Polymer 2003;44(14):3945–61.
[15] Fu BX, Yang L, Somani RH, Zong SX, Hsiao BS, Phillips S, et al. J Polym Sci, Part B: Polym Phys 2001;39(22):2727–39.
[16] Joshi A, Butola BS. Polymer 2004;45(14):4953–68.
[17] Ito M, Mizuochi K, Kanamoto T. Polymer 1998;39:4593.
[18] Bahr JL, Mickelson ET, Bronikowski MJ, Smalley RE, Tour JM. Chem Mater 2001;13:3823–4.
[19] Wang ZG, Wang XH, Hsiao BS, Andjelic S, Jamiolkowski D, McDivitt J, et al. Polymer 2001;42(21):8965–73. Andjelic S, Jamiolkowski D, McDivitt J, Fischer J, Zhou J, Wang ZG, et al. J Polym Sci, Part B: Polym Phys 2001;39(1):153–67.
[20] Lincoln DM, Vaia RA, Wang ZG, Hsiao BS, Krishnamoorti R. Polymer 2001;42(25):9975–85. Lincoln DM, Vaia RA, Wang ZG, Hsiao BS. Polymer 2001;42(4):1621–31.
[21] Liu ZJ, Yan DY. Polym Eng Sci 2004;44(5):861–7. Liu XH, Wu QJ. Eur Polym J 2002;38(7):1383–9.
[22] Kissinger HE. J Res Natl Stand 1956;57:217.
[23] Mitchell CA, Krishanamoorti R. Submitted for publication.
[24] Dobreva A, Gutzow I. J Non-Cryst Solids 1993;16:213–25.
[25] Koenig MF, Huang SJ. Polymer 1995;36:1877–82.